HiSST: 2nd International Conference on
High-Speed Vehicle Science & Technology

16–19 May 2022, Bruges, Belgium

Design space exploration for a scramjet engine by using data mining and low-fidelity design techniques

Ali Can Ispir [1], *Bora O. Cakir* [2], *Bayindir H. Saracoglu* [3]

Abstract

Scramjet propulsion systems offer seamless operation to the high-speed vehicles along their hypersonic flight phase without carrying on-board oxidizer or any rotating component. To discuss the reliability and feasibility of the entire system and trajectory, it is necessary to perform conceptual design exercises which are based on reduced-order approaches and enable one to investigate effect of multiple parameters. In this article, we created a multi-dimensional design space of a scramjet engine with five varying design variables which are flight Mach number and altitude, intake wedge angle and exit Mach number, and fuel-air equivalence ratio. We computed the intake and overall system performance parameters and implemented Artificial neural network regression technique into the dataset to perform comprehensive exploration the design space of the engine under investigation.

Keywords: *high-speed air-breathing propulsion, artificial neural network, scramjet, hypersonics*

1. Introduction

Ramjet and scramjet engines provide distinct advantages to their rocket counterparts for hypersonic propulsion because they do not either require on-board oxidizer storage or contain any rotating parts. The main distinction of scramjet engines over ramjet is that the flow keeps its supersonic character throughout the entire engine whereas, in ramjet engines, the incoming air flow is decelerated to subsonic conditions before the fuel is injected into it. Although the engine structure is simpler than turbo based aero-engines, there are multiple phenomenon which describe the flow complexity inside the propulsive duct and they should be well-investigated to make sure the system and flight trajectory reliability [1]. In this regard, the conceptual design methods based on zero-and-one dimensional approaches and preliminary performance analysis are considered as cost effective solutions as compared to expensive high-fidelity numerical and experimental methods. They basically analyze the impact of design parameters and operational variables of main system components and make performance estimation for given inputs such as in terms of thrust and fuel consumption [2, 3]. There are some efforts to build thermodynamic models which can solve the flow the ramjet/scramjet propulsive paths and make low-fidelity examination on the engine phenomenon. Zhang et al. coupled the one-dimensional inviscid flow equations with regenerative cooling to examine temperature and pressure rises in a scramjet duct and effect of heat transfer between the 1D supersonic flow and cooling channels placed around the combustor [4]. Torrez et al. developed a one dimensional model to investigate the precombustion shock and dissociation effects in a scramjet engine [5]. They examined the shock train structure in the isolator and combustor in three modes that are ram, early scram and late scram during the acceleration of the vehicle. Birzer and Doolan utilized a one-dimensional ODE set to model a hydrogen-fueled scramjet combustor and they validated their approach with Hyshot-II experimental case [6].

On the other hand, one of the major challenges in the scramjet engine design process is to make sure

[1] *PhD Candidate, VKI (von Karman Institute for Fluid Dynamics), Aeronautics and Aerospace Department, Chaussée de Waterloo 72, Rhode-Saint-Genese, ispir@vki.ac.be*

[2] *PhD Candidate, VKI (von Karman Institute for Fluid Dynamics), Turbomachinery and Propulsion Department, Chaussée de Waterloo 72, Rhode-Saint-Genese, cakir@vki.ac.be*

[3] *Research Expert, VKI (von Karman Institute for Fluid Dynamics), Turbomachinery and Propulsion Department, Chaussée de Waterloo 72, Rhode-Saint-Genese, saracog@vki.ac.be*

that the Mach number along the flow path is above than 1. Since the heat release and converged parts of the system decelerate the supersonic flow, the Mach number can possibly drop under the unity. This case is defined as thermal choke and causes several stability and performance issues. Therefore, engine parameters such as captured mass flow rate of the air and fuel consumption should be chosen carefully in the consideration of ambient conditions in order to both fulfill the trajectory requirements and avoid approaching the limits of the sonic condition [7]. The ambient i.e. flight conditions do not play important role only on the thermal choking phenomenon, but also they are very critical in the intake design and performance which is directly related with the overall system capabilities [8, 9, 10]. Additionally, the considerations of total pressure recovery factor, losses and startability issues at the intake, one dealing with the design and optimization of a scramjet is obliged to investigate plenty of design variables and parameters. This makes design process be more complicated and causes designers to tackle the problems when they want to portray the grand scheme of things. Because the multi-dimensionality of the design matrix does not allow to read the impacts of the variables on the performance and design parameters precisely with ease.

In the present work, we propose a methodology combining the reduced-order techniques and Artificial neural network regression model in order to explore the design space of a dual mode ramjet engine in scramjet operation. We create a data matrix including five independent design variables of the intake (wedge angle and exit Mach number), combustor (equivalence ratio) flight properties (altitude and Mach number). We compute propulsive performance parameters which are uninstalled thrust, specific impulse, fuel consumption, leftover fuel mass fraction and overall efficiency in each varying design parameter. Also we evaluate the intake design for given variables in the consideration of total pressure recovery, captured air mass flow rate, startability index and compression ratio. Each objective function is regressed by using the ANN method and a deep discussion is conducted for the intake and overall propulsive system performances in the framework of the relevant flow physics.

2. Methodology

2.1. Propulsive path design & analysis

2.1.1. Intake design and analysis module

The intake configuration is determined according to the design needs of a generic hypersonic cruiser with a fuselage integrated propulsive system. In consideration of the flow development over waveriders where the external aerodynamic characteristics are required to be in agreement with the flow topology of the propulsive flow path which demands an axisymmetric flow layout due to the structural integrity and performance requirements of combustion chamber [11]. Thus, the preliminary contouring of the scramjet intakes is based on inward tuning intake geometries with a converging nature [12]. Accordingly, due to the widespread applicability and modularity of its configurations, the intake geometry is described with three dimensional axisymmetric flow template of a Busemann diffuser [13].

$$\frac{du}{d\theta} = v + \frac{\gamma - 1}{2} uv \frac{u + vcot(\theta)}{v^2 - 1} \tag{1}$$

$$\frac{dv}{d\theta} = -u + (1 + \frac{\gamma - 1}{2} v^2) \frac{u + vcot(\theta)}{v^2 - 1} \tag{2}$$

The template for any axisymmetric, conical flow formation can be described by the streamtube shapes derived based on a two dimensional Taylor-Maccoll (T-M) flow [14] and it is shown that the validity of the T-M flow can be extended to a three dimensional space by means of a streamtube shape, called a Busemann flow [15]. Their mathematical description can be formulated by recasting the linearized first order T-M equations by the radial, u (Eq.1), and angular, v (Eq.2) Mach numbers [16]. The set of equations can be solved employing a numerical integration scheme of Runge-Kutta 4 (RK4)[17]. The initial condition for the integration is determined by the intensity of the terminating conical shock and the integration direction is from the exit of the intake, towards the freestream where the flow alignment with the horizontal axis is met.

The flow patterns observed for the designed family of high-speed intakes exhibit two main flow features. These appear in the form of isentropic compression and expansion regions, and oblique shock waves that either start or terminate the respective flow templates. Hence, in order to calculate flow field properties throughout those regions to determine the relevant performance specifications, two distinctive set of formulations are utilized. The flow property variations over the shock waves are calculated using the oblique shock wave relations [18] and fed into the respective flow characterization schemes. Moreover, the isentropic relations are employed to compute the flow properties throughout the isentropic expansion and compression regions [19].

2.1.2. Combustor analysis module

Furthermore, the flow development taking place in the combustor and the nozzle components is modelled by a quasi-one-dimensional set of governing equations coupled with detail-chemistry relations similar to the ones given in [4].

$$\frac{1}{\rho}\frac{d\rho}{dx} = \frac{1}{\dot{m}}\frac{d\dot{m}}{dx} - \frac{1}{U}\frac{dU}{dx} - \frac{1}{A}\frac{dA}{dx} \tag{3}$$

$$\frac{1}{U}\frac{dU}{dx} = \frac{-1}{\gamma M^2}\left(\frac{1}{p}\frac{dp}{dx} + \frac{2\gamma M^2 C_f}{D} + \frac{\gamma M^2(1-\epsilon)}{\dot{m}}\frac{d\dot{m}}{dx}\right) \tag{4}$$

$$\begin{aligned}\frac{dT}{dx} = \frac{1}{C_p}\Bigg(- \sum_i (h_i \frac{dY_i}{dx}) + [\frac{1}{\dot{m}}\sum_i \left(h_i(\frac{d\dot{m}_{i,added}}{dx})\right) - \frac{h_0}{\dot{m}}\frac{dm}{dx}] - \\ \frac{2C_f C_p(T_{aw}-T_w)}{Pr^{2/3}DA} - U\frac{dU}{dx}\Bigg)\end{aligned} \tag{5}$$

The fuel-air mixture was assumed to behave as an ideal gas and the state equation is given in Eq. 6.

$$\frac{1}{p}\frac{dp}{dx} = \frac{1}{\rho}\frac{d\rho}{dx} + \frac{1}{T}\frac{dT}{dx} - \frac{1}{\bar{MW}}\frac{d\bar{MW}}{dx} \tag{6}$$

As a result of the reaction and fuel addition, the change of molecular weight of the mixture is updated, Eq. 7.

$$\frac{d\overline{MW}}{dx} = -\overline{MW}^2 \sum_i \left(\frac{1}{MW_i}\frac{dY_i}{dx}\right) \tag{7}$$

Species equation is also implemented to find species mass fractions resulting from the reaction and injection processes, given in Eq. 8.

$$\frac{dY_i}{dx} = \frac{\dot{\omega}_i MW_i A}{\dot{m}} + \frac{1}{\dot{m}}\frac{d\dot{m}_{i,added}}{dx} - \frac{Y_i}{\dot{m}}\frac{d\dot{m}}{dx} \tag{8}$$

The mass gradient term $\frac{d\dot{m}_{i,added}}{dx}$ represents mass addition i.e. fuel injection to the system duct. However, since the fuel is assumed as ideally mixed with air stream in the entrance of combustion, this term is taken as zero in the solutions.

All transport equations and detailed chemistry coupling with the Arrhenius approach are defined as a set of ordinary differential equations (ODE). The reaction rates are calculated by a detailed chemistry mechanism including 33 reactions among 13 species [20]. The thermophysical properties of each species are computed with the data supplied by JANAF thermochemical tables [21]. A stiff ODE solver that can operate in different time scales is necessary to solve the present problem. As also suggested in [4],

the SUNDIALS (Suite of Nonlinear and Differential/Algebraic Equation Solvers) code [22], developed by Lawrence Livermore National Laboratory was chosen for the iterative solution of this problem. CVODE solver among other six solvers in the code is capable of solving initial value problems defined with stiff or non-stiff ODE systems. In the version of Sundials 2.6.2, the CVODE solver can be accessible in MATLAB environment. To deal with this mathematical stiffness problem, a non-linear Newtonian solver accompanied with backward differencing approximations was selected.

2.1.3. Nozzle analysis module

The same transport equations in the combustor module are also solved for the inviscid flow in the nozzle. Accordingly, the flow exiting the combustion chamber is perfectly expanded to the ambient conditions through a contoured nozzle [23]. Nevetheless, in accordance to the efficiency and performance specifications exploited for hypersonic cruise [24], Summerfield criteria conditioning the minimum nozzle exit pressure is higher than 30% of atmospheric pressure is taken into account in the performance examination [25]. Since the ambient pressure varies in a wide range of the flight altitude in the present problem, the overexpansion is not inevitable for many samples. Hence, the nozzle length variable becomes important and will be discussed later with the performance parameters in the framework of aforementioned criteria.

2.2. Propulsive database of the scramjet engine

The design space of the scramjet engine under investigation in the present work was created with input parameters given in Table. 1. The design variables are shown in fig. **??**a. The objective functions which are total pressure recovery at the intake, captured air mass flow rate, startability index, uninstalled thrust, specific impulse, fuel consumption and unburnt hydrogen mass fraction were computed thanks to the modules detailed above with given inputs. This paved the way for a compherensjove discussion about the impacts of the input parameters on the engine performance.

Table 1. The design variables range of the scramjet engine under investigation

Variables	Range
Cruise Mach number (ϕ_1)	[6 - 8]
Cruise Altitude [km] (ϕ_2)	[25 - 35]
Equivalence ratio (ϕ_3)	[0.14 - 0.5]
Wedge angle (ϕ_4)	[0 - 8]
Pre-combustion Mach number (ϕ_5)	[1.3 - 4.5]

2.3. Artificial neural network

A database including 3350 observations, was generated by the reduced-order modules detailed above. It basically aims to generate surrogate model representing the scramjet engine performance as a function of the elevation, flight Mach number, intake wedge angle, fuel-air equivalence ratio and intake exit Mach number. The regression model in the present work is desired to build accurate mathematical pattern between these independent design variables and the performance parameters. For this purpose, as a regression method, we selected Artificial neural network (ANN) composing of interconnected network of neurons. A basic ANN architecture consisting of input layer, a number of hidden layers, and an output layer, is drawn in fig. 1. It basically aims to create a representative model by finding appropriate mathematical relations between the input and output layers to make accurate predictions on the points which are not explored in the simulations. By this way, we are enabled to explore entire design space of the engine under investigation.

As seen in fig. 1, the input layer comprises the independent design variables while output layer is chosen as the engine performance parameters in the current problem. The deep learning models were built on the Keras platform [26]. In the models, the information given by the independent variables are transferred via the neurons in the consecutive layers with weights, w, biases, b, and activation functions, f. The weights at the i^{th} neuron represents the impact of each input (a_i) on output a_{out}. The computation of an output from a neuron in the j^{th} layer, is given in eq. 9.

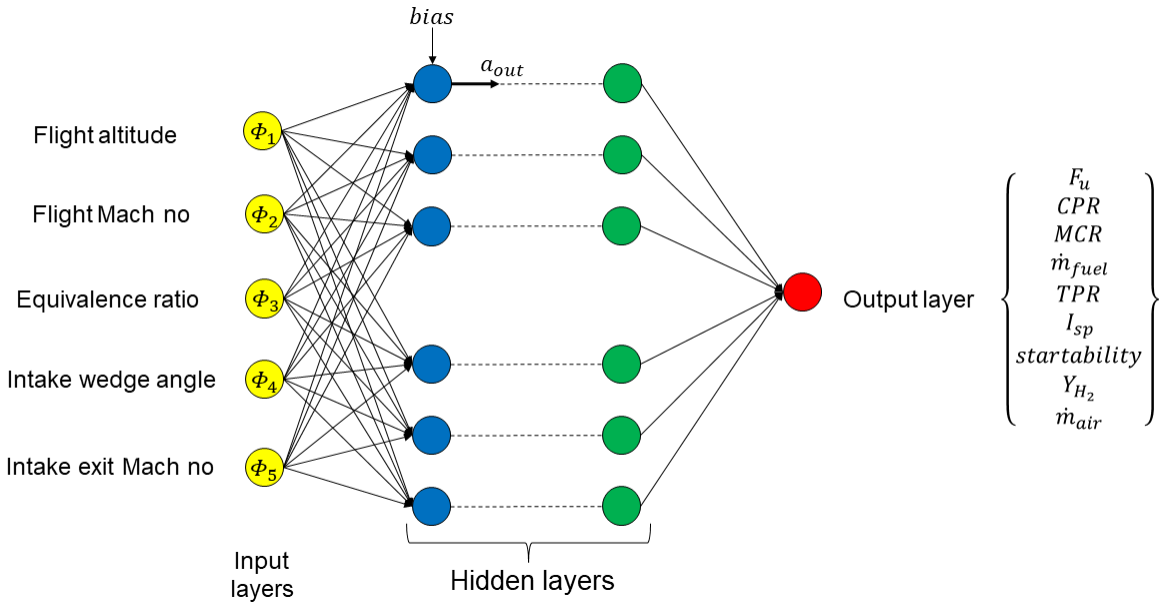

Fig 1. Schematic illustration of a deep neural network model built for the present problem.

$$a_{out} = f_j\left(b_j + \sum_i^N a_i w_i\right). \tag{9}$$

The number of layers, neurons in each hidden layer, learning rate, activation functions and also the scaling factors of the dataset are called as hyper-parameters of the regression model and the prediction performance significantly depends on their selection [27]. In order to optimize these parameters, Random search method [28] which is available in the Keras platform, is used to find the optimal hyper-parameters for each ANN model constructed in this work. For the regressions of all of the objective functions (engine performance parameters), rectified linear activation function (ReLU) showed better performance than other activation functions (such as sigmoid or hyperbolic tangent). Thus, we selected ReLU to activate hidden layers and activated output layer with a linear function. For determining the best scaling factor for the input parameters, a cost function, $\mathcal{L}$, proposed in the literature [29, 30] was utilized. This allowed us to find the best scaling factor which promises the best regressibility of each objective function. The individual costs $\mathcal{L}_i([\widetilde{\phi}_1, \widetilde{\phi}_2, \widetilde{\phi}_3, \widetilde{\phi}_4, \widetilde{\phi}_5], Fu, CPR, TPR, \dot{m}_{fuel}, I_{sp})$ were computed, where tilde denotes a scaled value. The scaling factor selected with this way to minimize the cost value $\mathcal{L}_i$, were noted in Table 2 in sec. 3.1. Each independent variable in the input matrix, ϕ_i, is divided by its standard deviation s in Auto scaling, by $\sqrt{s}$ in Pareto scaling, by $s^2/\text{mean}(\phi_i)$ in VAST scaling. The $\langle -1, 1 \rangle$ scaling scales each variable to the $\langle -1, 1 \rangle$ range.

The computation of the coefficient of determination, R^2, gives representative hint about the regression prediction performance. R^2 computations in each objective function regression are shown in the Table 2. However, since the overall R^2 can be misleading to make sure the regression performance accuracy, the dataset is divided into several bins (25-30), local errors are also depicted by the parity plots detailed in sec. . Equation 10 shows the calculation of the R^2 in the j^{th} bin. N_j represents the number of observations, $\phi^j_{o,i}$ and $\phi^j_{p,i}$ are observed and predicted outputs, respectively for the i^{th} dependent variable in the j^{th} bin.

$$R_j^2 = 1 - \frac{\sum_{i=1}^{N_j}(\phi_{o,i}^j - \phi_{p,i}^j)^2}{\sum_{i=1}^{N_j}(\phi_{o,i}^j - \text{mean}(\phi_o^j))^2}, \tag{10}$$

3. Results

3.1. Machine learning model and manifold assessment

The Artificial neural network (ANN) regression method was applied into the dataset created via the modules given in sec. 2.1. The ANN models were built to regress each objective function separately. The hyper-parameters of each model were optimized for the best prediction performance by using the Random Search class found in the Keras platform. The performance parameters related with the entire system which are uninstalled thrust F_u, specific impulse I_{sp}, fuel consumption $\dot{m}_{fuel}$, overall efficiency η_o, and unburnt hydrogen rate Y_{H_2}, were regressed by utilizing the five input parameters. However, for the simplification and decreasing the computational cost, ER variance was removed in the regression of the intake performance parameters which are CPR, ζ, $\dot{m}_{air}$, and startability index. As mentioned above, the machine learning models trained in this work by using the data created by the reduced order solutions, are expected to be a good representative of the scramjet engine design space and utilized during the design exercises of the propulsion system. Therefore, maximizing the prediction performance is quite essential, R^2 values were checked in each bin of each performance parameters regression. The global error rates are presented in Table. 2 with the optimized hyper-parameters of each ANN model while local errors are shown by using parity plots given in fig. 3.

Table 2. The optimized hyper-parameters of the Artificial neural network that yield the best R^2 value. The hyper-parameters are respectively: scaling factor, the number of hidden layers, cost for independent parameter optimization, $\mathcal{L}_i$, and the learning rate, α. We also show the overall R^2 values obtained for each objective function.

Obj. Fun.	Scaling	# Hid. lay.	$\mathcal{L}_i$	α	R^2
F_u	Auto	19	1.17	0.0001	.99
I_{sp}	Auto	15	1.25	0.0001	.99
$\dot{m}_{fuel}$	Auto	15	1.19	0.0001	.98
η_o	Level	12	1.26	0.0001	.99
Y_{H_2}	Level	5	1.32	0.0001	.97
$startability$	Vast	4	1.03	0.0001	.99
CPR	None	4	0.98	0.0001	.99
$\dot{m}_{air}$	Auto	10	1.15	0.0001	.99
ζ	Auto	9	1.17	0.0001	.99

The global and local errors respectively given in Table. 2 and fig. 3, indicate that the selected regression technique was capable to predict the data of F_u, $\dot{m}_{fuel}$, startability index, CPR, ζ, and $\dot{m}_{air}$ almost perfectly. The computed F_u data via the reduced-order solutions lies down between -0.1 and 8MN range. As will be discussed in next section, it was observed that the system produced more thrust with increase of the cruise Mach number. In the dataset, there is a distinct gap between the number of the observations obtained with flight speeds of Mach 6 and 8. The equivalence ratio range for the Mach 6 subdataset was selected as wider and investigated points are more frequent as compared to higher flight Mach numbers. The reason of paying more attention on the lowest investigated flight speed is to determine the thermal choking and non-combustion zone boundaries properly. Hence, an important part of the F_u data was aggregated mostly the range between negative values and 2MN. In the zone representing the thermal choking regime on the performance maps, F_u and accordingly I_{sp} and η_o, were calculated as 0 while they took negative values in the non-combustion zone since the propulsive path could not gain enough momentum increase. The nonlinear regression model had some difficulties to distinguish the independent variables which either cause the thermal choking or non-combustion

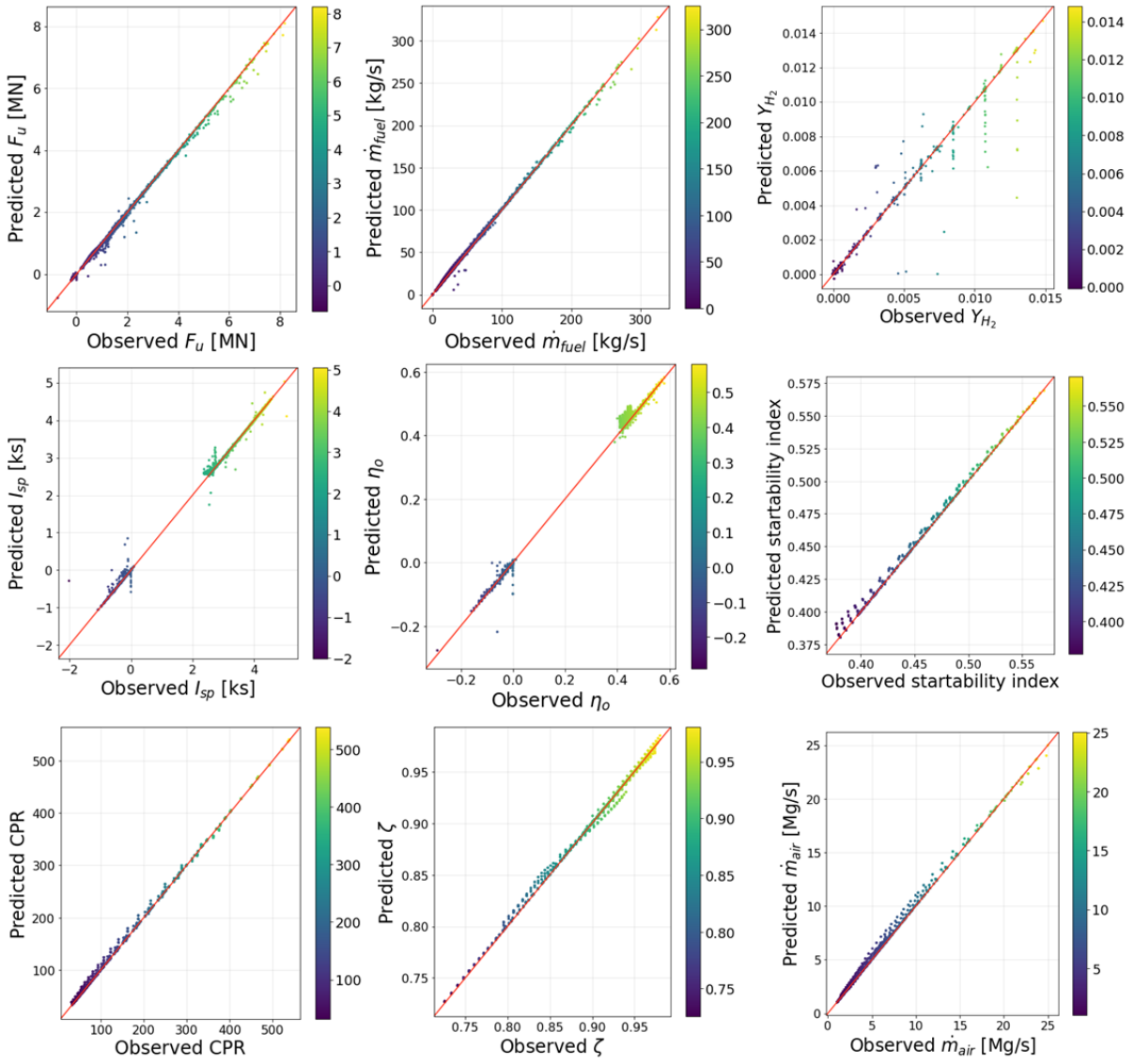

Fig 2. Parity plots of each objective functions predicted by the Artificial neural network regression model built correspondingly

regime. It could cope with the non-linearity of the dataset by increasing the complexity of the network i.e. requiring the high number of neurons and layers for instance in the objective functions of F_u and I_{sp}. This significantly increased the computational costs. Despite of the promising R^2 values, the deep learning model could not avoid confusing two phenomenon. In a small part of the dataset where the engine encounter thermal choking phenomena, the ANN model F_u was computed as negative since it presumed those points in the non-combustion region. Moreover, it can be also said since the I_{sp} was computed by the F_u and $\dot{m}_{fuel}$, its matrix includes both parameters non-linearity and this made the prediction more difficult. The similar expression can be hypothesized about the η_o. We thus, recommend to compute these performance parameters from the predicted F_u and $\dot{m}_{fuel}$ for such a database which is non-linear, complex and consists of multiple phenomena. Another remark can be made for the unburnt rate of hydrogen, Y_{H_2}. There are two main reasons for the leftover hydrogen: thermal choking where the fuel consumption stops because Mach number reaches unity, non-combustion where the hydrogen leaves the combustor without reacting. In the rest of the scenarios, in general, the Y_{H_2} was very close to zero. The ANN model constructed for this objective function failed to train the data when it took the values beyond 0.004. The non-linearity of aforementioned phenomenon were also contributed by the complexity of the combustion inside the duct and the model was not capable to make prediction every part of the design space. As it can be seen in fig. 3, the number of data around zone where the model is unsuccessful, are certainly less than the ones in other regions. The shortening the interval in the range of the independent design variables and performing more simulations at Mach 6 could be an option to improve the capability of the regression technique in terms of species mass fraction.

3.2. Scramjet performance

3.3. Intake performance

Performance specifications of the intakes operating at different cruise conditions and design parameters are analyzed by means of the flow properties extracted at the exit of the intake. The intake exit Mach number ($M_{I,E}$) and the leading edge truncation angle () are the two design parameters dictate the shape of the intakes for a given cruise Mach number. Accordingly, for constant leading edge truncation angle, decreasing $M_{I,E}$ increases compression pressure ratio. Although the total pressure recovery (TPR) reduces with decreasing $M_{I,E}$ due to the strengthening terminating conical shock, the unique geometry of the Busemann diffuser enables high efficiency compression of the incoming air. This is achieved by minimizing the compression performed through the terminating shockwave which is the main source of total pressure loss. On the other hand, increasing at constant intake exit Mach number decreases CPR due to increasing total pressure loss induced by the incidence shockwave attached to the leading edge. The geometric modifications introduced on the design procedure, which is governed by the flow Mach number and alignment at the upstream end of the Busemann diffuser, by means of varying the truncation angle is rather minimal. Thus, the terminal shock intensity is preserved while increasing rises the intensity of the incidence shock which in return reduces TPR. Nevertheless, as a portion of the compression is performed at the leading edge already, the deceleration required to slow down the incoming air to the desired pre-combustion properties is relaxed for the Busemann diffuser component which improves the startability characteristics of the intakes.

In terms of the influence of varying design parameters on mass flow rate (MFR), a strict dominance of CPR is observed. The aforementioned effect of changing the exit flow properties to meet the demands of combustion chamber on the static pressure development over the contours of the intake directly correlates with the resultant MFR. Elevating the exit flow velocity in terms of $M_{I,E}$ lowers the induced deceleration which reduces the level of compression performed by the intake. Even thought, at the exit of the intake static temperature rises with decreasing $M_{I,E}$, the effect of temeprature variation on MFR is overpowerd by the static pressure elevation. Hence, decreasing $M_{I,E}$ at constant leading edge truncation angle, yields the MFR values to rise. Whereas with increasing while the at constant $M_{I,E}$ degrades the mass flow capturing capabilities of the intakes which is quantified by a corresponding decrease in MFR.

Moving on to the effect of operating conditions in terms of altitude and flight Mach number, the intake performance is observed to change drastically even with constant design parameters over the designated operational range. Accordingly, increasing altitude is reducing the dynamic pressure the intake

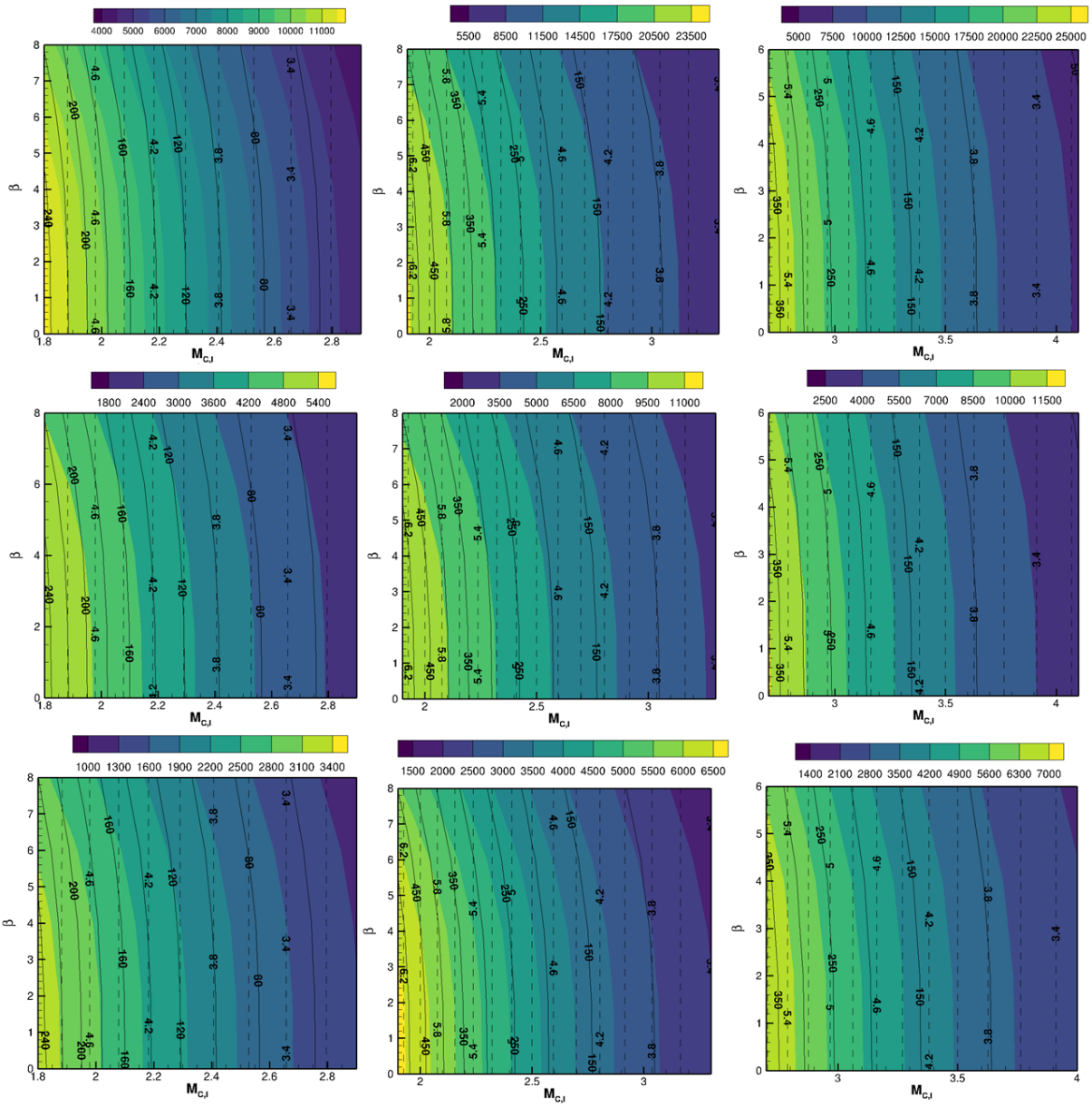

Fig 3. Mass flow rate (MFR in kg/s) maps of the intakes under investigation with varying leading edge truncation angle and intake exit Mach number for varying flight Mach number 6 - 8 (from top to bottom) and altitude 25 - 35km (from left to right)

is exposed to. The ratios of flow properties (TPR,CPR, TR) at the exit of the intake and at the inlet do not change with altitude since the intakes are design with a Mach number dependent methodology. Hence, variations in the cruise altitude don't introduce any modifications on the CPR range achieved by the intake. However, it reduces the mass flow rate through the intake which has a significant impact on startability. Thus, with increasing mass flow rate while the CPR range is kept constant, the startability is hindered which confines the operable design space of the intakes to provide feasible pre-combustion conditions. Additionally, the effect on temperature is purely adiabatic for varying operating conditions as the total temperature is preserved. Thus, the temperature ratio is kept constant as the cruise altitude is varied. Nonetheless, as the static temperature is altered with changing altitude, the corresponding pre-combustion temperature is modulated in relation to T_∞. On the other hand, changing flight Mach number and keeping the intake exit Mach number range constant, alters the temperature ratio. Hence, the flow at the inlet of the intake (freestream) entails a greater stagnation temperature which is converted to a higher static temperature values at the combustion inlet.

In accordance to the variations of CPR and TR induced by changing altitude, the mass flow rate of air entrained by the intake is drastically reduced as the altitude is increased. There are two main components affecting the value of the MFR at constant contraction ratio of the intake at constant the intake exit Mach number which are the local flow density and flow speed. Increasing the altitude lowers the static temperature which decreases the local speed of sound, thus the flow velocity at constant Mach number increases. Moreover, the density variations with altitude are mainly governed by the static pressure as modulations in the range of CPR overweights the ones in temperature ratio. Hence, the resulting effect on MFR is a rather significant reduction in comparison to lower altitudes. Varying the flight Mach number considerably alters the startability characteristics, as the operable range within the investigated design space is shifted towards higher intake exit Mach numbers as the flight Mach number is increased. Accordingly, the increasing exit Mach number of the intake allows higher CPR design points to start since the higher velocity of the exiting flow allows to overcome larger adverse pressure gradients. Referring to the aforementioned discussion on the dominance of CPR for determining the MFR through the intake, increasing allowable CPR (by self-startability constraints) enables a greater MFR to be accommodated by the intakes.

3.4. Propulsive performance

The propulsive performance of the investigated DMR engine operating scramjet mode are evaluated with uninstalled thrust F_u, specific impulse I_{sp}, fuel consumption $\dot{m}_{fuel}$, overall efficiency η_o, and unburnt hydrogen mass fraction Y_{H_2}. In this section, we also demonstrated the performance maps which enable to comprehend engine characteristics in the investigated design space.

One of the utmost important performance parameters F_u are influenced significantly by the independent variables under investigation in this present work. As seen in fig. 4, the higher Mach number flight caused the higher F_u to be produced by the propulsive unit. One of the main reasons is surely the $\dot{m}_{air}$ captured by the intake component. The $\dot{m}_{air}$ changes remarkably with the M_{CI} and it is worth to mention that M_{CI} ranges vary for the three investigated flight Mach number. For the same M_{CI}, elevation, and β, $\dot{m}_{air}$ is higher with the higher flight Mach number and this increases the computed F_u. On the other hand, the pre-combustion flow conditions provided by the intake computations are significant for the performance calculations. The CPR increases with the flight Mach number for the same M_{CI} and at the same altitude. The P_{CI} is slightly higher with the lower flight Mach number, despite of this, the F_u was computed higher as attributed to higher values of the $\dot{m}_{air}$. For the T_{CI}, there is no remarkable difference between the values with the increase of the flight Mach no. However, there are many points where the intake design failed to satisfy for the favorable pre-combustion flow conditions and the mixture entered the combustor with T_{CI}s under auto-ignition limit of hydrogen-air combustion. If the compression along the combustor is not enough to reach this limit, the mixture leaves the burner without combustion. These observation points are generally clustered around the high values of the M_{CI} for the specifically investigated cruise Mach number (fig. 4). This can be also interpreted that the selected design parameters for the intake component around these regions on the design maps, are not capable to provide the optimal initial flow conditions and the F_u values were computed negative due to the deficiency of the momentum increase (combustion) and aerodynamic losses.

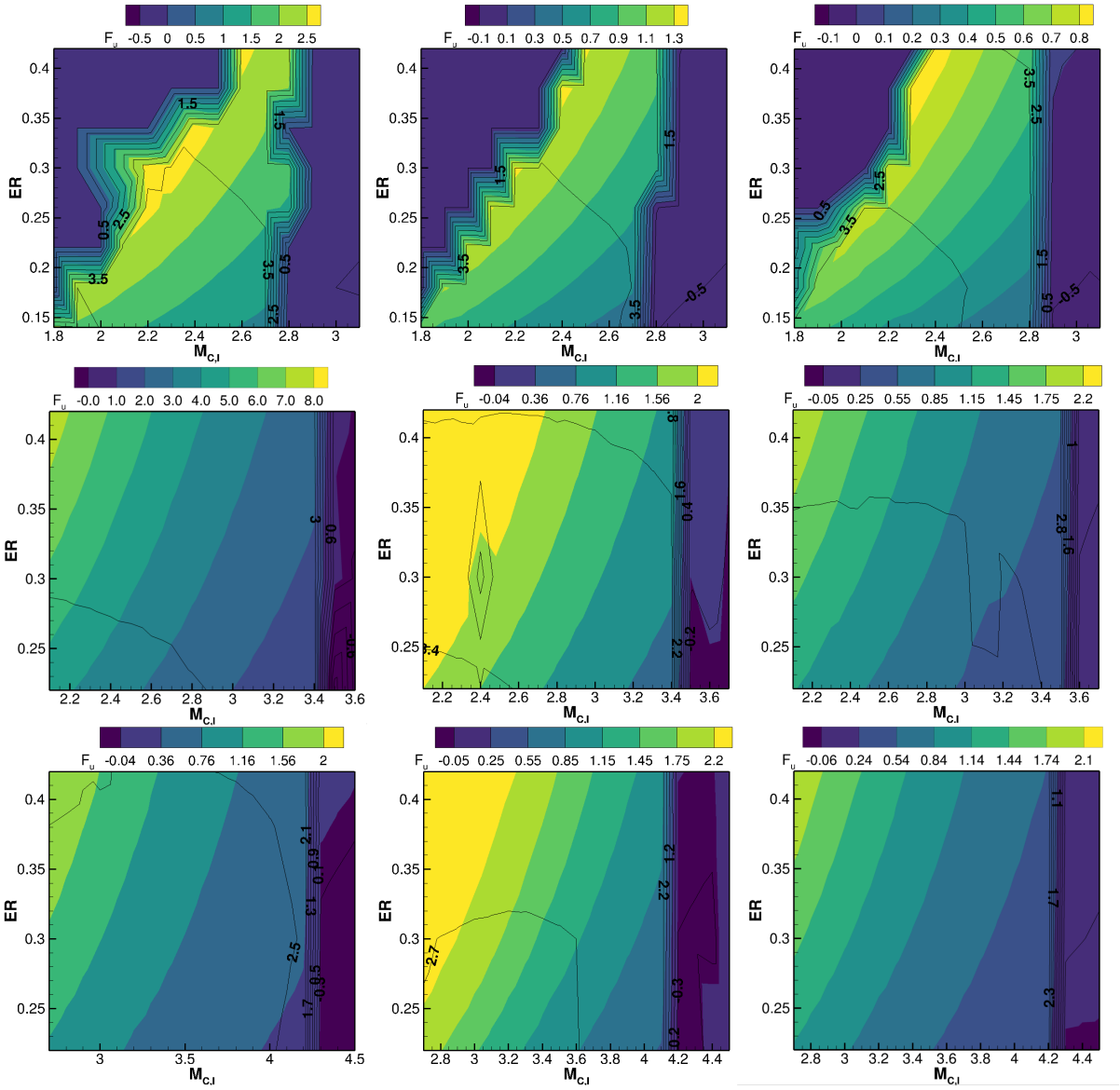

Fig 4. F_u [MN] maps of the propulsion system under investigation designed with 0 wedge angle scenario for varying flight Mach number 6 - 8 (from top to bottom) and altitude 25 - 35km (from left to right) (intersecting lines represent I_{sp} [ks])

The F_u showed an increasing trend with decreasing of M_{CI} and increasing ER for the cruise speeds of Mach 7 and 8. The curve of the F_u in the decreasing direction is cut by the M_{CI} limit of non-combustion. This indicates the limits of the operation range of these flight speeds in terms of the M_{CI}. However, for Mach 6 cruise investigations, the performance map is a bit different than the ones of the higher speeds. The operating zone is limited by two regions which are non-combustion one (high pre-combustion Mach number and insufficient compression at the intake) and thermal choke one. The thermal choke phenomenon is generally reasoned by selection of low M_{CI} and extreme compression at the intake. The great CPR does not only increases the losses along the propulsive duct but also, it caused the flow to decelerate more than optimal M_{CI} point and thermal choking is not inevitable in such cases. These regions represent two extremities, in one of them, the initial temperature is not enough to ignite the mixture while the heat addition (depending on the ER) might decelerate the flow under the sonic conditions in the other. The increase of the ER made the region of the thermal choking spread into the direction of increasing M_{CI} and the design space which can give promising F_u shrunk as seen in Mach 6 performance maps (fig. 4). As long as the mixture is not at the conditions of enough temperature, the increase or decrease of ER do not matter. It is worth to remind that the fuel is assumed to ideally mixed with air and be heated up to the same temperature of the air before the mixing in the present work. In general, the hydrogen is injected with lower temperature than the one of the air [31], this increases the gap between the mixture and auto-ignition temperatures and in such cases, M_{CI} is recommended to select by considering the heat transfer between the streams. The design of the scramjet flying at Mach 6 cruise conditions are very critical as considering these examinations. One ought to pay attention for the selection of the M_{CI} and ER (and accordingly $\dot{m}_{fuel}$) in order to avoid thermal choking and non-combustion zones.

For the investigated ER values in the current work, there is no thermal choke observed for the cruise speeds of Mach 7 and 8. Because the heat addition was not sufficient to decelerate the supersonic flow to the sonic conditions in the selected range. Moreover, the M_{CI} naturally is high enough not to even close to the thermal choking region. However, the higher ER investigations are suggested to be examined for determining the design limit of the engine in terms of the ER, and as indirectly $\dot{m}_{fuel}$. Similar remarks with the Mach 6 would be possibly observed.

Another independent variable implying that $\dot{m}_{air}$ is the dictating parameter for the F_u, is the flight altitude. The greater elevation decreases the F_u and one of the root causes is the significant drop of the captured $\dot{m}_{air}$. Flying at the different altitudes make also small changes on the limits of the thermal choking and non-combustion regions with respect to the M_{CI} and ER. The change of elevation is highly associated with the initial flow conditions and even a little change on the T_{CI} may alter the limit of these regions. The T_{CI} slightly rises with the increase of the elevation and this changes the limit of non-combustion a bit and push it to further in the axis of M_{CI}. For instance, for Mach 7 and 0.3 of ER operation, the limit is around 3.4 at 25 and 30km elevations while it becomes 3.5 if the altitude is selected 5km higher.

The P_{CI} values change remarkably with the flight altitude, but its impact is not as strong as the one of the $\dot{m}_{air}$. As also mentioned above, with the higher initial pressure, the higher F_u would be produced by the propulsion power plant. The P_{CI} and $\dot{m}_{air}$ along the M_{CI} axis followed opposite trend and the F_u showed the same trend with $\dot{m}_{air}$. This indicates the importance of the $\dot{m}_{air}$ for the engine performance. The intake wedge angle, β has influence on the F_u even though it is not as big as other parameters. It affects the engine performance via the captured $\dot{m}_{air}$ and ζ. The increase of the β causes the $\dot{m}_{air}$ and ζ at the intake to decrease slightly. These changes can be seen from the thrust calculations and it can be said that the selection of greater β made detrimental effect on the F_u. On the other hand, the higher β increased the T_{CI} and this resulted in the operation area of the thermal choking be reduced.

Specific impulse, I_{sp} is the measure of the thrust production per consumed fuel. In many simulations, I_{sp} curves follows a non-linear trend which is the combination of the ones of the $\dot{m}_{fuel}$ and F_u. The greater $\dot{m}_{air}$ is captured with the lower M_{CI} selection at the intake design. After a certain threshold of the M_{CI} depending on the investigated flight Mach number, it is not possible to produce thrust anymore since the favorable conditions cannot be provided for the auto-ignition of the hydrogen-air mixture. Therefore, we confronted the negative thrust and I_{sp} in the performance maps given in fig. 4. Except the non-

combustion region, I_{sp} increases in decreasing direction of M_{CI} for all investigated flight conditions. The increase rate decreases and after a while, it was observed to be insensitive to the selected M_{CI}. For a given flight Mach and altitude, the increase of $\dot{m}_{fuel}$ with the ER does not cause the same increment rate of the F_u for the same M_{CI} i.e. $\dot{m}_{air}$. Therefore, it was observed that the I_{sp} slightly decreases with the ER for all flight conditions under investigation. Moreover, the increasing of flight Mach number at the same altitude resulted in a dramatic increase of the $\dot{m}_{air}$. This increment means more consumed fuel for the same M_{CI} and since the engine thrust did not increase same with this, I_{sp} decreases remarkably with the increase of the cruise speed. Despite of the increases on the CPR and $\dot{m}_{air}$ with greater values of the cruise Mach number, F_u increase was not at the same rate with $\dot{m}_{fuel}$. On the other hand, the greater wedge angle selected at the intake design causes the aerodynamic losses as mentioned above. The decrease of the I_{sp} with the wedge angle can be linked to this examination. However, this detrimental effect of the greater wedge angle is not as big as the other parameters. Also, it is worth to say that the impact of the altitude was not found significant for the I_{sp}.

For the trajectory reliability, it is very essential to know the average fuel consumption and make sure the fuel tanks have enough capacity to provide designed $\dot{m}_{fuel}$ along the flight trajectory. The $\dot{m}_{fuel}$ strongly depends on the M_{CI} and investigated ER value. Along the M_{CI} range, $\dot{m}_{air}$ varies and $\dot{m}_{fuel}$ does not remain same with a given ER. Since the lower elevation flight causes the higher amount of air flow in-taken into the propulsive duct (due to the higher air density at ambient), the $\dot{m}_{fuel}$ increases oppositely with the flight altitude. The decrease on the captured $\dot{m}_{air}$ with the increase of the wedge angle caused the less fuel to be consumed for a given ER. This can be seen as another reason of the thrust decrease except the losses mentioned above. In the comparison of the observations obtained for Mach 7 and 8 flight speeds, $\dot{m}_{air}$ and accordingly $\dot{m}_{fuel}$ are higher for Mach 8 for the same ER and M_{CI}. Although the thrust is higher in the Mach 8 solutions, it does not follow the same increment rate of the $\dot{m}_{fuel}$ and thus, I_{sp} decreases considerably.

Overall efficiency η_o which is obtained with the multiplication of the propulsive and thermal efficiencies, is computed almost same (around 0.45) for all observations and it made plateau except the regions of thermal choking and non-combustion. The independent variables under investigation made differences on the thermal and propulsive efficiencies. When the engine losses from the thermal efficiency, it was compensated by the propulsive efficiency. Or if the propulsive efficiency is low, η_o remained same thanks to the high value of the thermal efficiency. Although the losses on the TPR attributed mostly to the greater selection of β, influenced the I_{sp}, η_o did not change significantly with the wedge angle.

The unburnt fuel mass fraction indicated with Y_{H_2}, is one of the engine performance parameters concerning about the environmental impacts. In some of the observation points (non-combustion), the hydrogen left the combustor without being burnt and this certainly affects adversely the engine performance. The presence of unburnt fuel is reasoned by the incomplete combustion (like in the thermal choking phenomenon) or non-combustion cases because of the inconvenient selection of the combustor initial conditions. Except these regions, the fuel was consumed almost totally in all investigated observation points. In the Mach 6 performance maps, the all fuel flow left the combustor without burning in the observations where the M_{CI} is selected as higher than 2.8 and 2.9 for the 25-30 and 35km elevations, respectively. So, the Y_{H_2} is directly determined by the independent variables playing important roles on the $\dot{m}_{fuel}$. On the other hand, an important part of the fuel remained when the thermal choke happens in the Mach 6 solutions. In thermal choking points, the Y_{H_2} is direct proportional to the ER while the mixture reaches the unity of the Mach number more easily with the lower M_{CI}. For the investigated ER ranges in the Mach 7 and 8 solutions, since there is no thermal choking is seen, the only reason of the existence of the hydrogen at the nozzle is non-combustion beyond a certain threshold of the M_{CI}.

4. Conclusion

In the present study, we carried out a comprehensive design space exploration of a dual mode ramjet engine operating in scramjet flight conditions. We investigated several design variables and flight conditions (which are flight altitude and Mach number, intake wedge angle, equivalence ratio and intake exit Mach number) impacts on the overall (which are uninstalled thrust, specific impulse, fuel consumption and thermodynamic efficiency) and component-based performance (which are compression ratio, total

pressure recovery factor, and captured mass flow rate of air (for intake), leftover hydrogen (for combustor)). We generated a propulsive database including 3350 observations and applied Artificial neural network regression technique to generate a machine learning based model to ease the design process of the propulsion system. We present the main conclusions and discoveries from the current work in below:

- For the investigated equivalence ratio and pre-combustion Mach number ranges, thermal choking phenomenon was only observed in the design space created for the flight speed of Mach 6. The zone locates close to the low limit of the initial Mach number and enlarges in the direction of increasing equivalence ratio.
- Another significant observation should be paid attention is non-combustion region. Selecting the exit Mach number as extremely high in the intake solutions led to the flow left the combustor without reaction. This increased the leftover hydrogen rate and adversely affect the propulsive performance and environmental characteristic of the engine.
- The uninstalled thrust had a increasing trend with the increase of the cruise Mach number and decreasing altitude. We observed that captured mass flow rate of the air and air density (related with the altitude) play very significant roles on the determining the propulsive performance. We observed that there is a direct proportion between the uninstalled thrust and fuel consumption. Hence, while the thrust increases, specific impulse remain same in majority of the observations made for the same flight Mach number and altitude.
- The hyper-parameters of the deep learning model were optimized by using Random search available in Keras platform. The Artificial neural network performed well in all intake performance parameters and gave reasonable prediction for the uninstalled thrust and fuel consumption. However, it was seen that more data is necessary to train the model not to distinguish thermal choking, non-combustion and effective thrust production zones on the performance maps.

Acknowledgments

This project has received funding from the European Union's Horizon 2020 research and innovation programme under grant agreement No 101006856.

References

[1] SNB Murthy and ET Curran. *Scramjet propulsion*. American Institute of Aeronautics and Astronautics, 2001. DOI: 978-1-56347-322-7.

[2] Jicheng Ma et al. "Control-oriented unsteady one-dimensional model for a hydrocarbon regeneratively-cooled scramjet engine". In: *Aerospace Science and Technology* 85 (2019), pp. 158–170. DOI: 10.1016/j.ast.2018.12.012.

[3] Lu Tian et al. "Quasi-one-dimensional multimodes analysis for dual-mode scramjet". In: *Journal of Propulsion and Power* 30.6 (2014), pp. 1559–1567. DOI: 10.2514/1.B35177.

[4] Duo Zhang et al. "Quasi-one-dimensional model of scramjet combustor coupled with regenerative cooling". In: *Journal of Propulsion and Power* 32.3 (2016), pp. 687–697. DOI: 10.2514/1.B35887.

[5] Sean M. Torrez et al. "Reduced-Order Modeling of Turbulent Reacting Flows with Application to Ramjets and Scramjets". In: *Journal of Propulsion and Power* 27.2 (2011), pp. 371–382. DOI: 10.2514/1.50272.

[6] Cristian H Birzer and Con J Doolan. "Quasi-one-dimensional model of hydrogen-fueled scramjet combustors". In: *Journal of propulsion and power* 25.6 (2009), pp. 1220–1225.

[7] M. G. Owens et al. "Thermal Choking Analyses in a Supersonic Combustor". In: *Journal of Propulsion and Power* 17.3 (2001), pp. 611–616. DOI: 10.2514/2.5785.

[8] Shuvayan Brahmachary and Hideaki Ogawa. "Multipoint Design Optimization of Busemann-Based Intakes for Scramjet-Powered Ascent Flight". In: *Journal of Propulsion and Power* 37.6 (2021), pp. 850–867. DOI: 10.2514/1.B38383.

[9] Chihiro Fujio and Hideaki Ogawa. “Physical insights into multi-point global optimum design of scramjet intakes for ascent flight”. In: *Acta Astronautica* 194 (2022), pp. 59–75. ISSN: 0094-5765. DOI: https://doi.org/10.1016/j.actaastro.2022.01.036.
[10] Feng-Yuan Zuo and Sannu Mölder. “Flow quality in an M-Busemann wavecatcher intake”. In: *Aerospace Science and Technology* 121 (2022), p. 107376. ISSN: 1270-9638. DOI: https://doi.org/10.1016/j.ast.2022.107376. URL: https://www.sciencedirect.com/science/article/pii/S1270963822000505.
[11] M. K. Smart. “Design of Three-Dimensional Hypersonic Inlets with Rectangular-to-Elliptical Shape Transition”. In: *Journal of Propulsion and Power* 15.3 (1999), pp. 408–416. DOI: 10.2514/2.5459.
[12] Faure J. Malo-Molina et al. “Three-Dimensional Analysis of a Supersonic Combustor Coupled to Innovative Inward-Turning Inlets”. In: *AIAA Journal* 48.3 (2010), pp. 572–582. DOI: 10.2514/1.43646.
[13] SANNU MOLDER and EDWARD J. SZPIRO. “Busemann inlet for hypersonic speeds.” In: *Journal of Spacecraft and Rockets* 3.8 (1966), pp. 1303–1304. DOI: 10.2514/3.28649.
[14] George Emanuel and M Gad-El-Hak. “Analytical Fluid Dynamics”. In: *Applied Mechanics Reviews* 54.4 (2001), B68.
[15] R. Courant and K.O. Friedrichs. *Supersonic Flow and Shock Waves*. Applied Mathematical Sciences. Springer New York, 1999. ISBN: 9780387902326. URL: https://books.google.be/books?id=QsxeC0QfYw8C.
[16] Sannu Mölder. “The Busemann Air Intake for Hypersonic Speeds”. In: *Hypersonic Vehicles*. Ed. by Giuseppe Pezzella and Antonio Viviani. Rijeka: IntechOpen, 2019. Chap. 5. DOI: 10.5772/intechopen.82736. URL: https://doi.org/10.5772/intechopen.82736.
[17] Hans Munthe-Kaas. “High order Runge-Kutta methods on manifolds”. In: *Applied Numerical Mathematics* 29.1 (1999). Proceedings of the NSF/CBMS Regional Conference on Numerical Analysis of Hamiltonian Differential Equations, pp. 115–127. ISSN: 0168-9274. DOI: https://doi.org/10.1016/S0168-9274(98)00030-0.
[18] V. Babu. “Oblique Shock Waves”. In: *Fundamentals of Gas Dynamics*. Cham: Springer International Publishing, 2021, pp. 103–119. DOI: 10.1007/978-3-030-60819-4_7.
[19] J.D. Anderson. *Fundamentals of Aerodynamics*. McGraw-Hill Education, 2010. ISBN: 9780073398105.
[20] Casimir J Jachimowski. “An analytical study of the hydrogen-air reaction mechanism with application to scramjet combustion”. In: (1988).
[21] Bonnie J McBride. *Coefficients for calculating thermodynamic and transport properties of individual species*. Vol. 4513. NASA Langley Research Center, 1993.
[22] Alan C Hindmarsh et al. “SUNDIALS: Suite of nonlinear and differential/algebraic equation solvers”. In: *ACM Transactions on Mathematical Software (TOMS)* 31.3 (2005), pp. 363–396.
[23] Ali C Ispir, Pedro M Goncalves, and Bayindir H Saracoglu. “Thermodynamic efficiency analysis and investigation of exergetic effectiveness of STRATOFLY aircraft propulsion plant”. In: *AIAA Scitech 2020 Forum*. 2020, p. 1108.
[24] Johan Steelant et al. “Achievements obtained for sustained hypersonic flight within the LAPCAT-II project”. In: *20th AIAA international space planes and hypersonic systems and technologies conference*. 2015, p. 3677.
[25] V Fernández-Villace, G Paniagua, and Johan Steelant. “Installed performance evaluation of an air turbo-rocket expander engine”. In: *Aerospace science and technology* 35 (2014), pp. 63–79.
[26] François Chollet et al. *Keras*. https://keras.io. 2015.
[27] G. I. Diaz et al. “An effective algorithm for hyperparameter optimization of neural networks”. In: *IBM Journal of Research and Development* 61.4/5 (2017), 9:1–9:11. DOI: 10.1147/JRD.2017.2709578.
[28] James Bergstra and Yoshua Bengio. “Random search for hyper-parameter optimization”. In: *Journal of Machine Learning Research* 13.2 (2012).
[29] Kamila Zdybał et al. “Cost function for low-dimensional manifold topology assessment”. In: *manuscript submitted to Scientific Reports* (2022). DOI: 10.13140/RG.2.2.12370.84164.

[30] Kamila Zdybał et al. “PCAfold: Python software to generate, analyze and improve PCA-derived low-dimensional manifolds”. In: *SoftwareX* 12 (2020), p. 100630. DOI: 10.1016/j.softx.2020.100630.

[31] Sean M Torrez et al. “Reduced-order modeling of turbulent reacting flows with application to ramjets and scramjets”. In: *Journal of propulsion and power* 27.2 (2011), pp. 371–382. DOI: 10.2514/1.50272.